ELSEVIER

Biomaterials 22 (2001) 2635–2646

Biomaterials

www.elsevier.com/locate/biomaterials

Electrochemical characterization and immersion corrosion of a consolidated silver dental biomaterial

H.J. Mueller[a,*], R.W. Hirthe[b]

[a]*Paffenbarger Research Center, American Dental Association Health Foundation, National Institute of Standards and Technology, Gaithersburg, MD 20899, USA*

[b]*College of Engineering, Marquette University, Milwaukee, WI 53233, USA*

Received 25 September 2000; accepted 11 December 2000

Abstract

A consolidated silver (CS) material, an alternative to dental amalgam, was studied for corrosion. Chemically precipitated silver particles were acid activated and pressure consolidated to a volume porosity of 25%. In selected tests comparisons were made between CS and melted and cast silver particles (MS), silver with a known mass fraction purity of 99.998% (FS), a silver-palladium alloy (SP), and a dispersed-phase amalgam (DA). Fusayama artificial saliva was used with controlled variations in pH, sulfide content, mucin content, and absorbed oxygen content. Electrochemical polarization, electrochemical impedance spectroscopy, and immersion methods were used. Results revealed differences in the zero current potentials $E(I = 0)$ from forward polarization between CS and MS (or FS) in deaerated solution. By superposition of the cathodic polarization curves, the area for CS was increased by 7.3 times and was enclosed within an outer shell of material 5.5 μm thick. Polarization resistance was significantly the highest for SP, followed in order by MS (or FS) and CS or DA. With scanning electron microscopy, CS was shown to be significantly more susceptible than MS to long-term immersion corrosion. The modeled equivalent electrical circuits for CS and DA involved a double layer capacitance, a charge transfer resistance, and an element attributed to adsorption. The active pore depth for CS from the transmission line model for porous solids revealed satisfactory agreement with polarization results. It is concluded that the corrosion susceptibility of CS in Fusayama solution, while similar to that for DA, is greater than it is for MS.

Keywords: Silver particle consolidation; Artificial saliva; Corrosion; Electrochemical polarization; Impedance spectroscopy

1. Introduction

Corrosion of metals involves an alteration in structure and properties due to dissolution, leaching, or oxidation that result in soluble and/or insoluble products. Physical, chemical, and/or electrochemical interactions between metal and environment are involved. For dental biomaterials, this situation is further complicated by the spontaneous formation of a thin biofilm.

A consolidated-silver-particle material for direct filling applications was developed as a potential alternative to dental amalgam [1]. Acid-activated silver particles are pressure consolidated at 37°C into a microstructure consisting of grains comprising consolidated silver particles that are interspersed with approximately 25% porosity. Clinically, consolidation is achieved with either hand techniques or with an automatic reciprocating device.

Silver cones in endodontically treated teeth showed corrosion in the form of moderate to severe pitting, crater formation, and limited notching [2–4]. Sulfur, nitrogen, and chlorine were detected from blackened deposits on corroded silver cones and in periapical tissues. Silver-cone corrosion products were identified as sulfides, sulfates, carbonates, and amine complexes. These products were highly cytotoxic in tissue culture studies. The galvanic coupling of silver cones with base metal posts and gold alloy crowns was shown to be the cause for endodontic treatment failure of some silver point restorations [5].

Consolidated silver was shown to be susceptible to sulfide tarnishing [6]. The corrosion of consolidated silver may be different from corrosion of other forms of silver, such as melted and cast silver. Consolidated silver

* Corresponding author. Tel.: +1-301-975-4344; fax: +1-301-963-9143.

E-mail address: herb.mueller@nist.gov (H.J. Mueller).

0142-9612/01/$ - see front matter
PII: S0142-9612(01)00004-7

contains porosity, localized induced strain energy, absorbed liquid within its pore structure, and possibly entrapped liquid from processing. Melted and cast silver contains negligible porosity, negligible absorbed liquid, no entrapped liquid from processing, and a homogeneous grain structure with minimal variations in induced strain energy. Even without compositional differences, microstructural and surface film differences can still influence the thermodynamics and kinetics for corrosion. The hypothesis to be tested was that the electrochemical behavior and immersion corrosion of consolidated silver is different from that of melted and cast silver.

2. Materials and methods

2.1. Alloys

Five materials were used, consolidated silver (CS), melted and cast silver (MS), silver with a known mass fraction purity of 99.998% (FS), silver–palladium alloy (SP), and dispersed-phase amalgam (DA).

2.1.1. Sample preparation

Silver particles were chemically precipitated from a silver fluorborate solution, passed through a # 200 mesh, and subsequently heat treated at 750°C for 2 h. Bulk specimens were processed by activating silver particles at 23–25°C with fluorboric acid by treating in succession with 350 ml of a 2.38 mol/l solution for 4 min, and then with 500 ml of a 0.48 mol/l solution for 1 min. Particle stirring with a motorized stir-rod at moderate speed was done for 1 min and 5 s, respectively. At completion of each treatment, the excess liquid was decanted. After the last treatment, the moist particles were transferred to a stainless-steel, mold/plunger device. CS disk samples measuring 15.9 mm diameter $\times 2$ mm thick were prepared by applying a load using a hydraulic press. Prior to testing, the disk faces were polished with (600, 1200, and 2400) grit SiC papers. Sonication for 2 min in distilled water and then in ethyl alcohol was followed by surface drying with a purified air blast. Selected samples for geometric density determination were desiccated until a constant weight was achieved. A density of $7.9 \pm 0.1 \times 10^3\ \mathrm{kg/m^3}$ was achieved when 150 MPa was applied during pressing for 2 min. This corresponded to the approximate density of specimens prepared with hand or automatic clinical consolidation techniques.

Melted and cast silver (MS) specimens of the same size were prepared by induction melting the precipitated silver powder and centrifugally casting it in a lost wax mold. After 15 min of cooling in air; the castings were water quenched. A silver with a known high purity was also used. Silver foil (FS) with a mass fraction purity of 99.998% (Alfa, Ward Hill, MA)[1] was punched into 15.9 mm diameter disks. Microscopy of polished and etched FS samples revealed the foil contained negligible porosity. Disks of SP composed of Albacast alloy, Jelenko, Armonk, NY, with a mass fraction of 70 Ag, 25 Pd, 5 Cu, In, Zn% were induction melted and cast in a similar manner as for MS, since an alloy of the SP type is known [7] to have improved corrosion resistance; selected tests compared SP to CS, MS, and DA. Disks of DA, composed of Dispersalloy amalgam, Johnson & Johnson, East Windsor, NJ with a mass fraction of 34.7 Ag, 9.0 Sn, 5.8 Cu, 0.5 Zn, and 50 Hg% were pressed in a stainless-steel mold with 14 MPa applied for 2 min to the plastic mass. An amalgam was included since CS is a potential alternative to amalgam. All disk faces were polished the same as for CS. The tests to follow used selected materials and solutions in order to provide comparisons between particular material–solution combinations.

2.1.2. Porosity and surface area determination

The pore volume density of CS was characterized with geometric (ρ_g) and true (ρ_t) densities. Calculation of ρ_g was from the specimen weight and dimensions, while ρ_t was from the specimen weight and volume determined with a helium gas micropycnometer (Quantachrome, Boynton Beach, FL). Open-pore- and closed-pore-volume densities were calculated from the difference between $\rho_t - \rho_g$ and between $\rho_{th} - \rho_t$, respectively, where ρ_{th} equaled the theoretical density of $10.4 \times 10^3\ \mathrm{kg/m^3}$. Open-pore surface area, pore size and distribution were obtained with the multipoint BET nitrogen adsorption technique (Autosorb™, Quantachrome, Boynton Beach, FL).

2.1.3. Surface preparation for microstructural analysis

For bulk microstructural characterization, consolidated silver was manually polished with SiC abrasive sheets (Fibrmet™, Buehler, Lake Bluff, IL) consecutively with 9, 3, and 1 μm grit sizes. To remove effects from a retained smear layer, polished surfaces were etched by immersion for several hours in an aqueous solution composed of 0.75 mol/l KCN and 0.20 mol/l $(NH_4)_2S_2O_8$, while being agitated.

2.2. Artificial saliva solutions

An artificial saliva referred to as Fusayama was used [8]. Its composition consisted of NaCl, KCl,

[1] Certain instruments and materials are identified in this paper in order to identify the experimental methods adequately. Such identification does not imply recommendation or endorsement by the National Institute of Standards and Technology, nor is it intended to imply that the materials or equipment identified are necessarily the best available for the purpose.

$CaCl_2 \cdot 2H_2O$, $NaH_2PO_4 \cdot H_2O$, $Na_2S \cdot 9H_2O$, and urea at concentrations of (6.8, 5.4, 5.4, 5.0, 0.021 and 16.7) mmol/l, respectively. At 25°C and as prepared, the pH and electrical conductance were measured to be 4.7 ± 1 and $5866 \pm 75\,\mu S$, respectively. As noted, the original composition contained sulfide, no mucin, and with an acidic pH of 4.7. In an attempt to better simulate human saliva, and to study the effect of only one variable at a time, most of the tests to follow modified the original composition. A saliva with a higher pH, and with and without sulfide and mucin were used in selected tests. Hence, Fusayama saliva with a modification in pH to 6.5 ± 0.1, containing 2.2 mmol/l $NaH_2PO_4 \cdot H_2O$ and 2.4 mmol/l Na_2HPO_4 $7H_2O$ was used. Modified Fusayama saliva at a $pH = 6.5 \pm 0.1$ with and without 0.021 mmol/l $Na_2S \cdot 9H_2O$, and modified Fusayama saliva without sulfide but with a mass fraction of 0.1% mucin were also used. All solutions were used at 24 ± 1°C shortly after preparation.

2.3. Open-circuit potential (OCP) and direct current polarization

Cyclic voltammetry between (−1.0 and 0.5) V vs. SCE at 10 mV/s and single-sweep potentiodynamic polarization between −0.5 and 0.4 V at 1 or 0.17 mV/s were obtained in air-exposed, deaerated, or aerated artificial saliva. An EG & G Princeton Applied Research electrochemical cell, flat specimen holder, high-density graphite counter electrode, saturated calomel reference electrode (SCE), luggin probe, and potentiostat (model 273A) were utilized. The 15.9 mm diameter disk specimens were inserted into the flat specimen holder and a geometric area of 100 mm^2 of the sample face remained exposed. Current densities for the polarization plots were obtained by dividing current by the apparent exposed area of 100 mm^2, instead of by the total area calculated later in this paper. A computer was interfaced with the potentiostat via an IEEE-488 (GBIP) board, and control of the experiments was by version 352 corrosion measurement and analysis software (EG & G).

Solutions deaerated by purging with argon provided electrochemical measurements with minimized interference from dissolved atmospheric oxygen, while solutions aerated by purging with oxygen simulated clinical conditions. Solutions purged with argon for 2 h or oxygen for 30 min, prior to insertion of the alloy electrodes into the closed electrochemical cell, were taken to approach steady-state solution conditions. The open-circuit potentials (OCP) or corrosion potentials (E_{corr}) were measured for the first hour after the electrodes were inserted into the cell. Polarization experiments were mostly run at 1 mV/s, although selected experiments were run at 0.017 mV/s to find out if scanning rate affected differences between OCP and the zero-current potential upon forward potential scanning $E(I = 0)_f$. The slope of the forward polarization curves within ±5 mV from $[E(I = 0)]_f$ was used for determination of polarization resistance (R_p). Polarization curve slopes representing both reduction (β_{red}) and oxidation (β_{ox}) were also obtained. Forward polarization curve slopes at $E(I = 0)$ for calculation of R_p, and β_c and β_a, were determined with the software program. Arbitrariness in β_{red} and β_{ox} measurements was minimized by taking (i) the linear region, if any, apparent on the E vs $\log i/A$ plot, or (ii) the region of the plot with the highest value that modeled a linear fit. Three runs for each condition were made and the means and standard deviations presented. Tukey's comparison of the means test was performed at an $\alpha \leqslant 0.05$.

2.4. Immersion corrosion

CS and MS disk specimens, with the same specifications as those prepared for the electrochemical tests were immersed in 50 ml of artificial saliva at pH = 4.7 without sulfide and mucin, and contained in glass weighing bottles with a glass ground stopper. The contents were stored at 24 ± 1°C for 100 d. Three runs were made for each material. Throughout the first day of immersion, the samples were removed from solution, excess water blotted away, and weighed on an analytical balance with a resolution of 0.0001 g.

2.5. Impedance spectroscopy

Electrochemical impedance spectroscopy [9,10] characterized the complex impedance ($Z*$) at the CS and DA, and artificial saliva interfaces. For a parallel combination of a resistance (R) and a capacitance (C),

$$Z^* = R/(1 + j\omega\tau), \tag{1}$$

or

$$Z^* = R/(1 + \omega^2\tau^2) - j\omega\tau R/(1 + \omega^2\tau^2), \tag{2}$$

where $j = (-1)^{1/2}$, $\omega = 2\pi f$, f is the frequency in Hz, and $\tau = RC$ the time constant. Since the first and second terms in Eq. (2) represent the real part (Z') and the imaginary part (Z'') of $Z*$,

$$Z^* = Z' - jZ'' \tag{3}$$

A Solartron model 1260 impedance/gain-phase analyzer was interfaced with an EG & G model 273A potentiostat and controlled by Z_{plot}/Z_{view} software from Solartron (Scribner Associates, Inc., Charlottesville, VA). A sinusoidal signal of 25 mV was superimposed on the signal of the open-circuit potential. Measurements were begun at 10^4 Hz and terminated at 10^{-2} Hz. $Z*$ data points were collected at approximately 40 selected frequencies. The real component (Z') vs the imaginary component (Z'') of $Z*$ at all frequencies were plotted. A lumped parameter approach, consisting of single-valued resistances and capacitances was partly used to model an equivalent

electrical circuit to the impedance plots. The "constant phase element" accounted for dispersion of the electrical response away from single-valued resistances and capacitances. The circuit element used to describe such a response is denoted Q^n, where $n(0 \leqslant n \leqslant 1)$ indicates the degree to which the dispersion deviates from an ideal capacitance ($n = 1$) or an ideal resistance ($n = 0$). The complex impedance becomes

$$Z^* = R/(1 + j\omega\tau)^n, \quad (4)$$

where τ is the time constant $= (RQ)^{1/n}$. Software programs using nonlinear least-squares methods were used to test the fit of the selected equivalent electrical circuit to the impedance plots [11]. The goodness-of-fits were obtained by a χ^2 factor and a relative error term.

2.6. Surface analysis

Scanning electron microscopy (SEM) (JEOL, JSM-5300, Tokyo, Japan) and conventional energy dispersive spectroscopy (EDS) (IXRF Systems, Inc, Iridium, Houston, TX) analyses were performed on selected surfaces. For the immersion-tested samples, the disk faces directly exposed to the solutions were analyzed. Prepared samples were mounted with carbon tape on SEM aluminum stubs. For EDS, a tube voltage of 15 or 25 kV was used. X-rays were collected for a total of $200–210 \times 10^3$ counts with a Si crystal detector with a Be window. For semi-quantitative analysis, a standardless analysis with atomic number, absorbance, and fluorescence (ZAF) corrections was used.

2.7. Statistical analysis

Means and standard deviations ($\pm$) are presented in the tables of results to follow. For particular properties presented in the rows in Tables 1–3, Tukey's pairwise comparison of the means test at an $\alpha \leqslant 0.05$ was run amongst the different groups (columns). Means within the same row with the same superscript letter are not significantly different.

Table 1
Electrochemical properties (mean $\pm$ standard deviation)*

Property	Consolidated silver (CS)		Melted silver (MS)	
	Deaerated	Aerated	Deaerated	Aerated
OCP or E_{corr}, 1 h (mV)**	80 ± 10^{a}	85 ± 13^{a}	83 ± 9^{a}	79 ± 15^{a}
Potentiodynamic polarization				
Forward $E(I = 0)_f$ (mV)	48 ± 35^{bc}	24 ± 40^{b}	-150 ± 32^{a}	-31 ± 17^{ab}
Breakdown potential E_φ (mV)	96 ± 4^{a}	$110 \pm 13a^{b}$	103 ± 4^{ab}	115 ± 9^{b}
Reverse $E(I = 0)_r$ (mV)	81 ± 4^{a}	87 ± 8^{a}	92 ± 6^{a}	98 ± 8^{a}
Charge passed from				
$E(I = 0)_f$ to E_φ ($\mu C/cm^2$)	78 ± 11^{a}	151 ± 139^{a}	48 ± 20^{a}	49 ± 37^{a}
$E(I = 0)_f - 0.4\,V - E(I = 0)_r$ (mC/cm^2)	526 ± 67^{b}	485 ± 72^{ab}	466 ± 38^{ab}	423 ± 13^{a}
$E(I = 0)_r$ to $-0.32\,V$ (mC/cm^2)	541 ± 67^{b}	503 ± 81^{ab}	462 ± 37^{ab}	429 ± 15^{a}
Polarization resistance				
R_p ($k\Omega\,cm^2$)	80 ± 77^{ab}	32 ± 17^{a}	$590 \pm 140^{©}$	146 ± 55^{b}
Polarization slope				
β_{ox} (V/decade)	0.08 ± 0.04^{a}	0.16 ± 0.04^{b}	$0.43 \pm 0.18^{©}$	$0.42 \pm 6^{©}$
β_{red} (V/decade)	$0.82 \pm 0.20^{©}$	0.13 ± 0.01^{a}	0.44 ± 0.06^{b}	0.11 ± 0.02^{a}

*In Fusayama saliva, no sulfide, pH = 6.5, 1 mV/s, $n = 3$. Data in rows with the same letter are not significantly different at an $\alpha \leqslant 0.05$.

Table 2
Effect of sulfide on electrochemical properties (mean $\pm$ standard deviation)*

	CS		FS	
	Without sulfide	With sulfide	Without sulfide	With sulfide
OCP (mV)	80 ± 10^{b}	61 ± 26^{b}	80 ± 8^{b}	-194 ± 44^{a}
$E(I = 0)_f$ (mV)	48 ± 35^{c}	4 ± 28^{c}	-161 ± 27^{b}	-220 ± 23^{a}
E_φ (mV)	96 ± 4^{a}	120 ± 7^{b}	99 ± 4^{a}	126 ± 4^{b}
β_{red} (V/decade)	0.82 ± 0.20^{c}	1.80 ± 0.35^{d}	0.50 ± 0.02^{b}	0.21 ± 0.05^{a}

*In deaerated saliva, pH = 6.5, with and without 0.021 mmol/l $Na_2S \cdot 9H_2O$, 1 mV/s, $n = 3$.

Table 3
Effect of mucin on electrochemical properties (mean ± standard deviation)*

Property	CS*		FS*	
	Without mucin	With mucin	Without mucin	With mucin
R_p (kΩ cm^2)	32 ± 17^a	101 ± 23^b	198 ± 33^c	136 ± 38^{bc}
E_φ (mV)	110 ± 13^a	133 ± 11^b	113 ± 7^a	134 ± 3^b

*In aerated saliva, no sulfide, pH = 6.5, with and without a mass fraction of 0.1% mucin, 1 mV/s, $n = 3$.

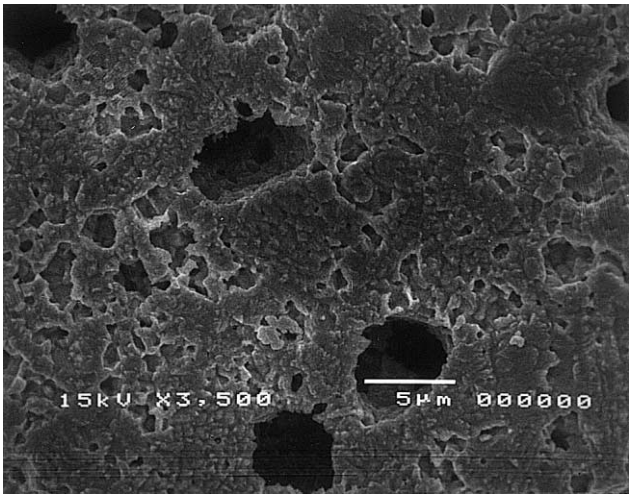

Fig. 1. SEM micrograph of the etched microstructure of consolidated silver.

3. Results

3.1. Structure characterization

Geometric density, pycnometer density, total pore area, mean pore diameter and pore volume less than 3.2 μm in diameter characterized pore structure. For CS and MS, the mean ± standard deviation ($n = 3$) for the pore properties listed in the above order were 7.94 ± 0.10 and 10.36 ± 0.10, 10.28 ± 0.02 and 10.45 ± 0.01 g/cm^3, 4.29 ± 0.01 and $0.28 \pm 0.01 \times 10^{-1}$ m^2/g, 0.22 ± 0.02 and $0.33 \pm 0.02 \times 10^{-1}$ μm, and 23 ± 0.01 and $2.0 \pm 01 \times 10^{-4}$ cm^3/g, respectively.

For CS, weight increased and plateaued after 24 h, while for MS negligible weight gain occurred. After 24 h, the mean relative mass gains for CS and MS were 0.812 and 0.004%, respectively. For CS the etched microstructure is presented in Fig. 1. Both larger pores, about 5 μm in size, and sub-micron sizes are revealed.

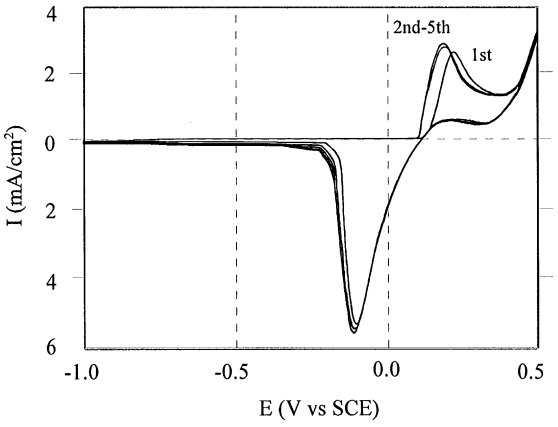

Fig. 2. Cyclic voltammetry at 10 mV/s of consolidated silver immersed in air-exposed Fusayama solution at a pH = 4.7 without sulfide.

3.2. Direct current polarization

3.2.1. Voltammetry

Fig. 2 presents the cyclic voltammetry (I/A vs E) for the first 5 cycles of CS in air-exposed saliva. The anodic scans revealed oxidation currents commencing at 0.09 V, while the cathodic scans revealed reduction currents commencing at 0.12 V. Replotting the voltammogram with an increased current density sensitivity by 2000 times still revealed the presence of only one oxidation and one reduction peak. The areas beneath the oxidation segments and the reduction segments of the curves represented the amount of oxidized and reduced charge passed, respectively. For the 2nd through 5th cycles the oxidation charge passed between 0.09 and 0.50 V upon forward potential scanning and between 0.50 and 0.12 V upon reverse potential scanning was 87.5 ± 1.1 mC/cm^2, while the reduction charge passed between 0.12 and -0.21 V was 77.1 ± 2.6 mC/cm^2. The 1st cycle showed lower anodic and cathodic charges by 10–12%.

3.2.2. Single sweep polarization

Figs. 3a and b present the anodic polarization curves (E vs $\log I/A$) for CS and MS exposed to deaerated and aerated saliva, respectively. Polarization for FS was similar to that for MS. Electrochemical properties associated with CS and MS in Figs. 3a and b are presented in Table 1. The OCPs for CS and MS in aerated and deaerated solutions were not significantly different. All zero-current potentials with forward potential scanning $E(I = 0)_f$ were lower than their OCPs. For MS in deaerated saliva, $E(I = 0)_f$ was significantly lower than for CS. Continued cycling beyond the 1st cycle maintained a significant distinction in $E(I = 0)_f$ between MS and CS. At 0.017 mV/s, $E(I = 0)_f$ for MS in deaerated saliva was still significantly lower than for CS. The breakdown potentials, E_φ, for CS and MS in aerated saliva were higher by 12–14 mV although not significantly, than in deaerated

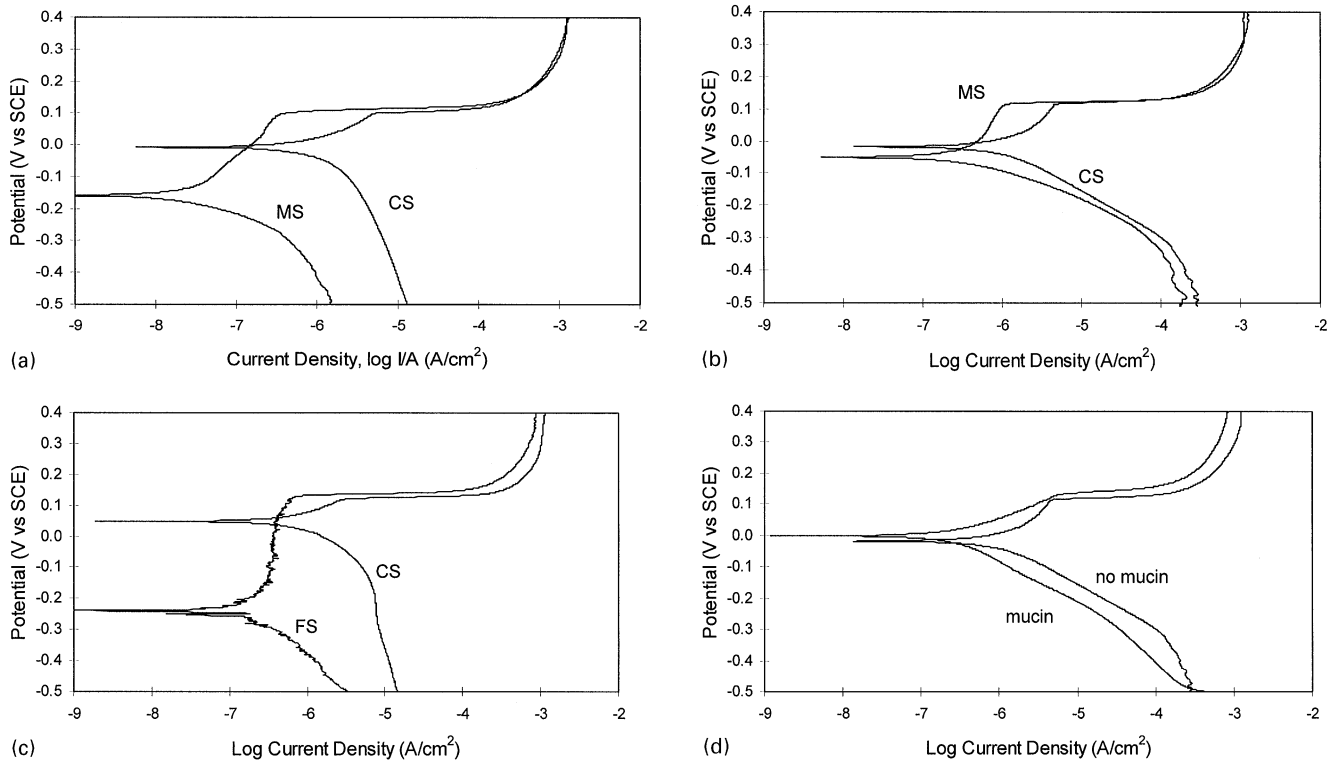

Fig. 3. (a) Anodic polarizations at 1 mV/s in deaerated Fusayama solution at a pH = 6.5 without sulfide. CS = consolidated silver and MS = melt-cast silver. (b) Anodic polarizations at 1 mV/s in aerated Fusayama solution at a pH = 6.5 without sulfide. CS = consolidated silver and MS = melt-cast silver. (c) Anodic polarizations at 0.17 mV/s in deaerated Fusayama solution at a pH = 6.5 with sulfide. CS = consolidated silver and FS = foil silver. (d) Anodic polarizations at 1 mV/s of consolidated silver in aerated Fusayama solution at a pH = 6.5 with and without a mass fraction of 0.1% mucin.

saliva. The zero-current potentials with reverse potential scanning $E(I=0)_r$ for CS and MS were similar. The amount of charge passed between $E(I=0)_f$ and E_φ was lower, although not significantly, for MS than for CS. The total oxidation and reduction charges passed for CS and MS in deaerated solution were higher, although not significantly, than for aerated solution. Determination of polarization resistance R_p for MS in deaerated saliva was significantly the highest, followed in order by MS in aerated saliva, CS in deaerated saliva, and by CS in aerated saliva. The slope for MS(β_{ox}) was significantly higher than for CS in either aerated or deaerated saliva. The reduction polarization curve slope β_{red} for CS and MS in deaerated saliva were significantly higher than for aerated saliva. For deaerated saliva, β_{red} for CS was significantly higher than for MS.

3.2.3. Material vs polarization resistance

Determination of polarization resistances R_p with a scanning rate of 1 mV/s for alloys exposed to sulfide-free mucin-free aerated saliva at a pH = 6.5 were as follows from the lowest to the highest. For CS, DA, MS, and SP, R_p was 32 ± 17, 38 ± 7, 146 ± 55, and $465 \pm 98\,k\Omega\,cm^2$. R_p was significantly the highest for SP, followed in order by MS, then by CS and DA, with the latter two representing one statistical group.

3.2.4. Effect of sulfide

Polarizations of CS and FS in deaerated saliva with the recommended concentration of sulfide are shown in Fig. 3c. As in Figs. 3a and b, MS and FS polarizations were similar. Figs. 3a and b show MS, while Figs. 3c and d show FS. Selected electrochemical properties for CS and MS in saliva with and without sulfide are listed in Table 2. Sulfide-containing saliva significantly decreased the OCP and $E(I=0)_f$ for FS (or MS) and increased E_φ for both materials, while β_{red} decreased for FS (or MS) but increased for CS. Aerated Fusayama saliva was not tested due to the instability from oxygen-induced sulfide degradation [12].

3.2.5. Effect of mucin

Polarization of CS in aerated saliva with and without a mass fraction of 0.1% mucin is shown in Fig. 3d. Selected electrochemical properties for CS and FS (or MS) are listed in Table 3. The effect of mucin also significantly increased R_p for CS, and E_φ for both CS and FS. For polarization in mucin-containing saliva, CS and FS (or MS) contained blackened surfaces, while surfaces polarized in mucin-free saliva were light gray. Besides, the morphology of the corrosion products formed without mucin and with mucin was different. Without mucin, tiny globules of products about 0.2 μm in diameter were

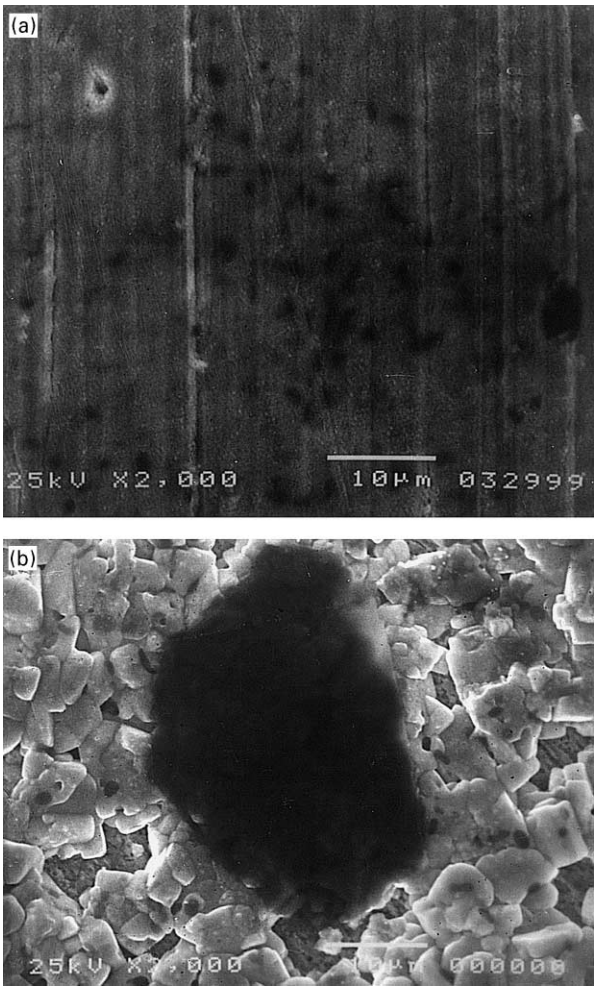

Fig. 4. (a) SEM micrograph of a polished surface of melt-cast silver particles after continuous immersion for 100 d in Fusayama solution at a pH = 4.7 without sulfide. The original polishing lines are detected along with occasional dark spots, related to the original retained porosity. EDS detected only Ag. (b) SEM micrograph of a polished surface of consolidated silver after continuous immersion for 100 d in Fusayama solution at a pH = 4.7 without sulfide. The surface is covered with a porous layer of Ag and Cl containing corrosion products, identified to be predominantly AgCl. Occasional black regions were thought to contain Ag_2O products. Gaps occur in the corrosion layer exposing underlying Ag.

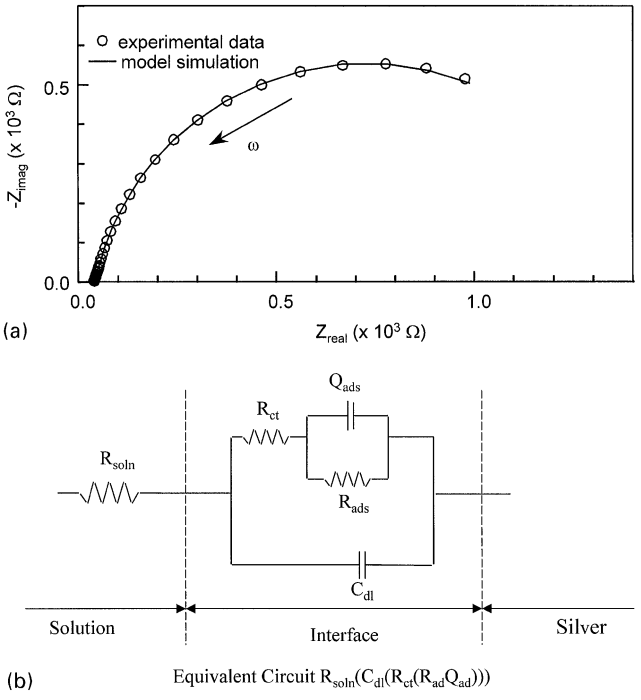

Fig. 5. (a) Complex plane impedance plot for consolidated silver exposed to air-exposed Fusayama solution at a pH = 4.7 without the added sulfide. The data points represent the experimental results, while the solid line represents the simulation of the equivalent circuit model shown in Fig. 5b. (b) Equivalent circuit model for consolidated silver and dispersalloy amalgam saliva interfaces.

joined into larger clumps about 1 μm in size. The incomplete joining of the larger clumps of material produced an irregular thick layer with irregular sized pores. With mucin, a denser layer occurred. The small globules were unified into a flattened layer with circular openings scattered throughout.

3.3. Immersion corrosion

Figs. 4a and b are SEM micrographs of the surfaces of MS and CS, respectively, after the 100 d immersion. MS showed negligible corrosion, while CS showed a porous layer of products covering the surface. For MS, EDS detected only Ag, while for CS, both Ag and Cl were detected, and semi-quantitatively correlated with AgCl. Black patches of products, overlaying CS were thought to be Ag_2O. The dark spots on the MS surface were associated with retained pores and were mainly confined to the central area of the disk face.

3.4. Impedance spectroscopy

An impedance plot for the interface between CS and air-exposed saliva without sulfide, pH = 4.7, after several days of solution conditioning, is shown by the data points in Fig. 5a. Results showed conditioning to solution provided for improved reproducibility. The data followed a near semicircular shape, but an exact match with a concentric semicircle did not occur. Fitting the experimental data points with nonlinear least squares (NLLS) to resistances (R) and capacitances (C) generated a model simulation of $R_{soln}(C_{dl}(R_{ct}(R_{ads}Q^n_{ads})))$, shown by the solid line in Fig. 5a. A schematic of the equivalent circuit is shown in Fig. 5b. An uncompensated solution resistance (R_{soln}), a double layer capacitance (C_{dl}), a charge transfer resistance (R_{ct}), and a resistance (R_{ads}) and a constant phase element (Q^n_{ads}) related to adsorption

Table 4
Component values for equivalent circuit $R_{soln}(C_{dl}(R_{ct}(R_{ads}Q^{n}_{ads})))$

Material	Component[a]							
	R_{soln}	C_{dl}	R_{ct}	R_{ads}	Q_{ads}	n	C_{ads}[b]	τ_{ads}[b]
CS	41	207	21	1369	483	0.80	435	0.60
Error[c]	0.2	2.8	8.5	0.6	1.2	0.4	—	—
DA	9	51	244	5717	101	0.73	82	0.47
Error[c]	1.4	1.1	8.9	2.7	1.8	1.3	—	—

[a] R in ohms (Ω,) C and Q in microfarads (μf), n is dimensionless, and τ in seconds (s).
[b] $(R_{ads}Q_{ads})^{1/n} = R_{ads}C_{ads} = \tau_{ads}$.
[c] Residual error in % between model prediction and experimental data.

comprised the model. For CS and DA, Table 4 presents results for the modeled circuit elements.

4. Discussion

4.1. Direct current polarization

4.1.1. Voltammetry

Cyclic voltammetry showed only one oxidation and one reduction peak, attributed to $Ag + Cl^- = AgCl + e^-$, even with the current density increased in sensitivity by 2000. Hence, CS did not show contamination from the stainless-steel mold and plunger during pressure consolidation at 150 MPa. Also, the existence of distinct oxidation/reduction phenomena from possibly retained fluorboric acid was not shown. However, any effect from possibly retained fluorboric acid on the Ag/AgCl couple was inconclusive from only the one scan presented.

Since the voltammetry was obtained in air-exposed saliva, the delayed behavior of the 1st cycle compared to the (2nd–5th) cycles was attributed to the effect of dissolved O_2 in solution. The cyclic repeatability of the conditioned electrode was excellent, confirming the chemical homogeneity of the surface layers. Furthermore, the cathodic/anodic charge efficiency of 0.80 demonstrated the high reversibility for the Ag/AgCl couple. During clinical applications, changes in E_{corr} occur due to changes in salivary biochemistry. Hence, as the potential fluctuates anodically and cathodically, AgCl surface films are in a state of continual formation followed by partial dissipation, respectively.

4.1.2. CS vs MS polarization

The experimentally determined polarization curves shown in Figs. 3a–d are external polarization curves, and do not explicitly represent the reactions for only the anode and the cathode. The OCP or E_{corr} and $E(I=0)_f$ correspond to mixed potentials, which include effects from the equilibrium potentials and polarizations for the anode (E_a) and the cathode (E_c). Theoretical polarization curves for the anode and the cathode are required to model the real corrosion behavior. This is the basis for the graphical solution to the multielectrode [13,14], and is used to represent corrosion processes alone or in combination under activation, mass transport, ohmic, or passivation control.

Since significant differences occurred for CS and MS between the OCP and $E(I=0)_f$ at scanning rates of 1 and 0.17 mV/s, scanning rates slower than 0.17 mV/s are required for steady-state conditions. Although the effects of cathodic polarization starting at -0.5 V and with scanning rates of 1 or 0.17 mV/s resulted in $E(I=0)_f \neq$ OCP, the fact remains that $E(I=0)_{CS} \neq E(I=0)_{MS}$. This distinction showed that electrochemical reactions and/or kinetic processes were different between CS and MS.

By maintaining the single-electrode equilibrium potentials of $(E^{\circ}_{red})_{MS} = (E^{\circ}_{red})_{CS}$ and $(E^{\circ}_{ox})_{MS} = (E^{\circ}_{ox})_{CS}$, and by using the experimental results of $(\beta_{ox})_{CS} < (\beta_{ox})_{MS}$ and $(\beta_{red})_{CS} > (\beta_{red})_{MS}$, a graphical interpretation of $E(I=0)_{CS} > E(I=0)_{MS}$ can not be made. Since CS and MS are pure Ag, their oxidation reaction $Ag = Ag^+ + e^-$ must be the same, or $(E^{\circ}_{ox})_{MS} = (E^{\circ}_{ox})_{CS}$. However, their anodic polarizations are different, as shown by differences between $(\beta_{ox})_{MS}$ and $(\beta_{ox})_{CS}$. By considering $(E^{\circ}_{red})_{MS} < (E^{\circ}_{red})_{CS}$, a graphical model can be constructed by extrapolation of their anodic and cathodic polarization curve slopes, as shown in Fig. 6. Qualitatively, agreement with experiment is made. Hence, the corrosion current $(i_{corr})_{CS} > (i_{corr})_{MS}$. The model suggests that differences occurred with reduction on CS and MS. Alternately, Fig. 6b presents a graphical representation where an ohmic potential drop (IR) is associated with the anodic polarization process for CS. Since $(E^{\circ}_{red})_{CS} - (E^{\circ}_{ox})_{CS} = ((E_{ox})_{IR} + IR) + (E_{red})_{IR}$, where $(E_{ox})_{IR}$ and $(E_{red})_{IR}$ are the differences in potential between the single-electrode equilibrium potentials and the potentials on the corresponding polarization curves at current density $(i_{corr})_{IR}$. E_{corr} is shifted positively by an amount equal to IR. For an ohmic drop associated with the reduction process, E_{corr} would be shifted negatively.

The pore structure of CS could have changed the composition, concentration, and conductivity of the electrolyte, and induced salt film formation [15–17] thereby increasing the ohmic resistance for the anodic process to occur. Also, because of possible retention of fluorboric acid from acid consolidation, species like $(H_3O\text{–}BF_3)^+$ must be considered (see below).

Because CS contained a pore structure (Table 3), the apparent surface area did not represent the true active area involved in electrochemical reactions. Taking the cathodic processes for MS and CS to involve 1 electron, an estimate of the active surface area for CS was obtained. Multiplying the polarization curve for CS shown

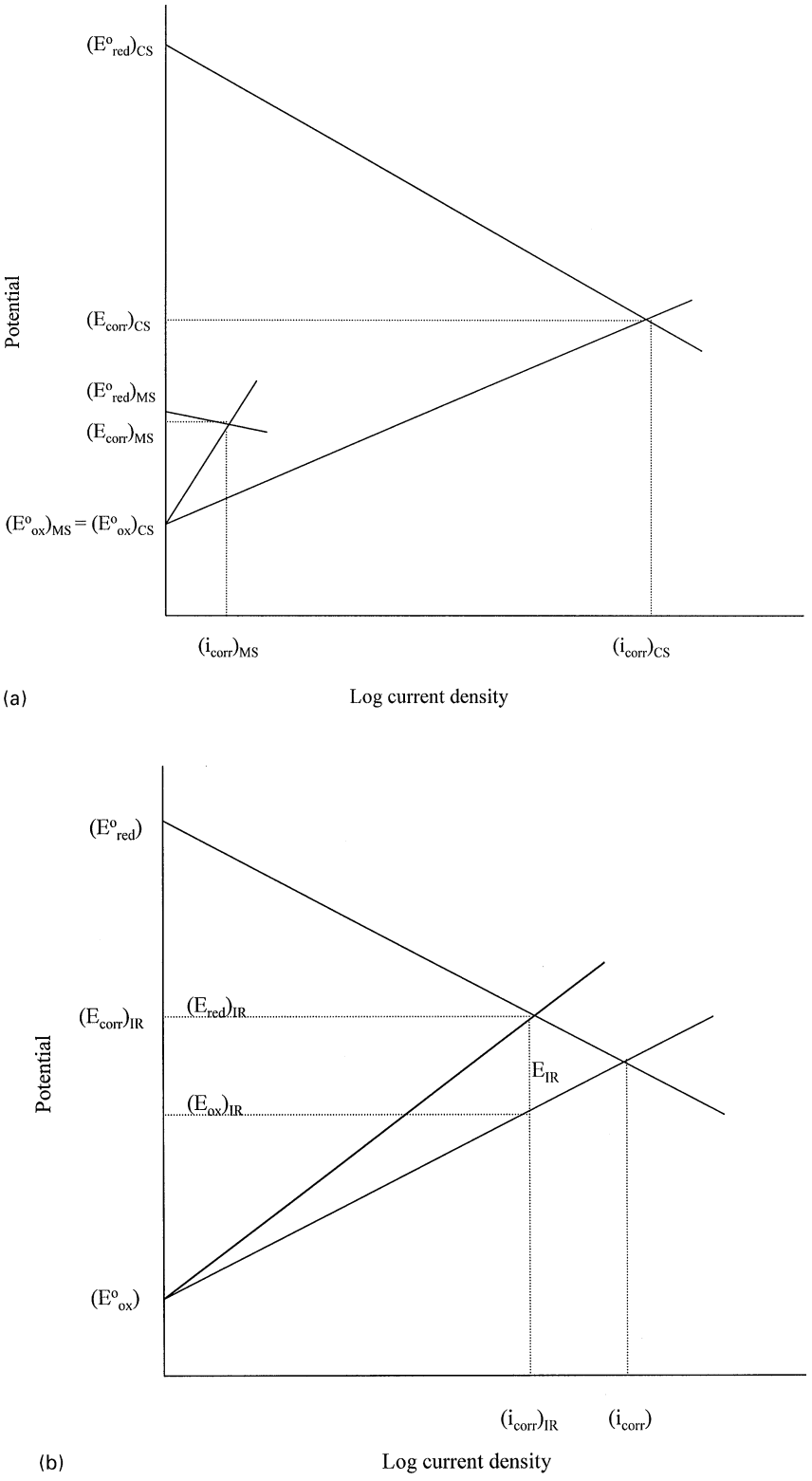

Fig. 6. (a) Model for the mixed potentials of consolidated silver (CS) and melt-cast silver (MS) in deaerated Fusayama solution. The slopes are in relative agreement with the measured polarization curve slopes. (b) Model for the mixed potentials of consolidated silver partially under ohmic control. The IR potential drop is taken to be associated with the oxidation process.

in Fig. 3a by a factor of 0.12 resulted in shifting the cathodic Tafel region near -0.5 V, to the same position as that for MS. This inferred that 8.3 cm^2 instead of 1.0 cm^2 was responsible for the electrochemistry of the CS sample. For all samples the mean active electrochemical area, A_{mean}, equaled 7.4 ± 4.3 cm^2. By normalizing A_{mean} to the total geometric surface area of a sample (dia = 15.8 mm and $t = 2.0$ mm) and dividing by the total pore surface area (Table 3), a pore surface area fraction of 0.0027 was obtained. This meant 0.27% of the total pore surface area was involved in the electrochemistry. Assuming the pore volume was distributed uniformly throughout the sample, only pores within 5.5 μm of the surface were involved in the electrochemistry.

4.1.3. Zero-current potential

Because $E(I=0)_{CS} \neq E(I=0)_{MS}$ differences in the soluble and insoluble corrosion products were suggested. Soluble pre-state compounds in solution are connected with the starting point of polarization (E_{corr}) and extend by 0.1 V and more to the potential associated with formation of solid corrosion products [18]. For pure Ag in Fusayama saliva, a potential range of 0.084 V existed between E_{corr} and the potential for the onset of solid AgCl formation [8]. Thus, the current density increase in the polarizations for CS and MS was due to the reaction, $Ag + Cl^- = AgCl + e^-$. The next solid compound to form was Ag_3PO_4 at a potential of 0.437 V and higher, and could not have occurred on CS or MS, since polarization ceased at 0.40 V. However, effects from the soluble pre-states of Ag_3PO_4 may have affected the polarization below 0.40 V. An explanation for the difference between $E(I=0)_{CS}$ and $E(I=0)_{MS}$ is formation of soluble pre-state compounds prior to the potential for solid product formation. MS revealed appreciable soluble AgCl compound formation, while CS showed limited soluble compound formation.

The distinction in $E(I=0)$ between CS and MS only existed in deaerated saliva. In aerated saliva, the process became that of $O_2 + 2H_2O + 4e^- = 4OH^-$ with $(E^\circ)_{O_2} = 0.401$ V (SHE). Reduction occurred with less resistance in aerated saliva as shown by the cathodic polarization slopes of 0.12 V/decade for both CS and MS. Under O_2 control, the region associated with pre-state AgCl soluble compound decreased in potential magnitude for MS and increased for CS, with $E(I=0)$ for both not being significantly different.

4.1.4. Saliva with sulfide

In Fusayama solution, solid Ag_2S forms at -0.485 V [8]. $E(I=0)_{FS,MS}$ and $E(I=0)_{CS}$ were favorable for solid Ag_2S formation. The instability of sulfide even in deaerated Fusayama saliva, as indicated on the polarization curve for FS and MS, may have prevented lower zero-current potentials. In deaerated Fusayama solution, $E(I=0)_{FS,MS}$ significantly decreased by 59 mV when sulfide was used, while $E(I=0)_{CS}$ was not significantly different with and without sulfide. This suggested that FS (or MS) was more reactive than CS to sulfide. The increase in $(\beta_{red})_{CS}$ to 1.8 V/decade indicated diffusion control. Ag_2S was the predominate product. Hence, the supply of the depolarizing ion was controlling. The decrease in $(\beta_{red})_{FS,MS}$ to 0.21 V/decade indicated improved kinetics for reduction. Pre-state soluble sulfide compounds occur below -0.485 V and would have been present soon after the start of polarization at -0.5 V. Solid Ag_2S formed prior to soluble and solid AgCl. Hence, a combination of products contributed to increasing the difference in saliva with sulfide between $E(I=0)_{FS,MS}$ and $E(I=0)_{CS}$ to 200 mV and more and contributed to the differences in the kinetics for reduction. These same factors may have also contributed to increasing E_φ for FS (or MS) and CS in sulfide-containing saliva.

4.1.5. Saliva with mucin

Since various silver oxides are black and/or plum, it appeared that mucin-containing saliva generated corrosion products of AgO, Ag_2O, or Ag_2O_3 in combination with AgCl, while mucin-free saliva generated corrosion products mainly composed of AgCl. Occlusion of the submicron-sized pore structure of CS by the larger-sized glycoproteins appeared related to the increased R_p for CS in mucin-containing saliva. Protection of the underlying CS substrate appeared more favorable with mucin. Also, the proteins delayed both CS and FS (or MS) from increrases in current density, since E_φ for both was significantly increased.

4.1.6. Retention of fluorboric acid

While the open pores made up most of the pore network, long-term retention of acid is more likely within the closed pores. However, outward diffusion and loss of possibly retained acid over time is more feasible from the open pores and their effect on corrosion is possible. If HBF_4 is initially retained, additional reactions are possible [19]. The reaction $HBF_4 = HF + BF_3$ converts to acid and boron trifluoride, with the boron trifluoride hydrating to basic complexes due to the following reactions of (i) $2BF_3 + 3H_2O = BF_3 \cdot H_2O + BF_3 \cdot 2H_2O$, (ii) $2(BF_3 \cdot H_2O) = (H_3O\text{–}BF_3)^+ + (BF_3OH)^-$ and (iii) $BF_3 \cdot 2H_2O = H_3O^+ + (BF_3OH)$. Reduction of cathodic regions by $(H_3O\text{–}BF_3)^+$ may be possible, while basic complexes of $(BF_3OH)^-$ may alter the corrosion reaction of Ag with the formation of products of $AgBF_3OH$. Corrosion could be increased, further supporting the differences in polarization between CS and MS.

4.1.7. Adsorbed films

Besides films formed with chloride, sulfide, and mucin, films formed with phosphate and urea must be con-

sidered. Calcium phosphate forms on titanium surfaces [20], so its formation on CS may also be possible. With dental amalgam, phosphate is known to produce both an inhibitory effect and a corrosive effect [21]. For CS, compound formation of phosphate could only be with silver cations. Ag_3PO_4 is a yellow insoluble compound [19]. Although solid Ag_3PO_4 formation is not thermodynamically feasible in Fusayama below 0.4 V [8], soluble pre-states of Ag_3PO_4 may have occurred. As for urea ($NH_2C{=}ONH_2$), metallic complexes with organic compounds, peptides, proteins, etc. have been well characterized with spectrometric techniques [22]. Silver coordination to a urea molecule is expected through silver binding to one or both amine NH terminal ends. Formation of a surface film of AgNHC=ONHAg may have occurred. Future work is required to ascertain this hypothesis.

4.2. Impedance spectroscopy

4.2.1. Equivalent electrical circuit

The simplest equivalent circuit model for a metal/solution interface is composed of a resistance and capacitance in parallel and characterized by a concentric semicircle. The real impedance is related to charge transfer resistance for oxidation and reduction (R_{ct}), and the capacitance from the imaginary impedance related to an electrical double layer resulting from adsorbed water molecules and hydrated cations (C_{dl}). The slightly flattened semicircular impedance plot determined for CS and DA can be modeled by two RC circuits, represented as two semicircles with equal diameters and centers separated along a line below and parallel to the real impedance axis [9]. For CS and DA interfaces, the second RC element with time constant τ was interpreted to be due to the phenomena of adsorption at the interface. Using Fusayama saliva without sulfide and mucin, an adsorbed film of possibly phosphate or urea complex with silver cations was involved. The uncompensated solution resistance (R_{soln}), an RC parallel circuit and an RQ parallel circuit were modeled as $R_{soln}(C_{dl}(R_{ct}(R_{ad}Q_{ad})))$, as shown in Fig. 5b instead of as two parallel elements in series $R_{soln}(C_{dl}R_{ct})(R_{ad}Q_{ad})$, since significantly less error with a nonlinear least-squares fit was obtained [11].

4.2.2. CS pore depth

Based upon a transmission line model for a porous electrode with penetration depth (λ in cm) much less than pore depth, $\lambda = (r_o R_p \times 10^{-6}/\rho)^{1/2}$, where r_o is the pore radius in μm, R_p is the polarization resistance, and ρ is the electrolyte resistivity [15]. Substituting $r_o = 0.011\,\mu m$, $R_p = 1.5 \times 10^3\,\Omega\,cm^2$ and $\rho = 170\,\Omega\,cm$ (1/0.005866), a penetration depth of 31 μm is obtained, which is in satisfactory agreement, considering these assumptions, with the 5.5 μm thickness obtained from polarization curve considerations.

In view of the model developed for a porous amalgam electrode [23,24], it is interesting that n for CS (0.80) was similar to n for DA (0.73). The porous nature of the CS electrode should have lowered the value of n, however, product deposition after immersion for several days before recording the impedance data may have occluded the interconnecting pores. The impedance plots showed improved reproducibility after the electrode was exposed to solution for at least a day. Hence, the impedance data may be characterizing the products on the surface and those occluding the pores instead of its pore structure. When data from additional CS electrodes with different pore contents are obtained, a better account of the CS impedance data can be made. If the spectra for CS do indeed characterize the pore structure, then the data will support the model that an amalgam corrodes via a porous film [23].

5. Conclusions

Besides composition, microstructure also affects corrosion. Because of the porosity and microstructural heterogeneity with consolidated silver, it is concluded that the corrosion of consolidated silver is greater than that of melted and cast silver.

Acknowledgements

This work was supported by the American Dental Association Health Foundation, National Institute of Standards and Technology, and by the USPHS Research Grant P50 DE 09322 from the National Institute of Dental and Craniofacial Research, National Institutes of Health, Bethesda, MD.

References

[1] Lashmore DS, Dariel MP, Johnson CE, Ratzker MB, Giuseppetti AA, Eichmiller FC, Beane GL, Kelly DR. Acid assisted cold welding and intermetallic formation and dental applications thereof. US Patent No. 5711866, 1998.
[2] Seltzer S, Green DB, Weiner N, DeRenzis F. A scanning electron microscope examination of silver cones removed from endodontically treated teeth. Oral Surg 1972;33:589–605.
[3] Brady JM, del Rio CE. Corrosion of endodontic silver cones in humans: a scanning electron microscope and X-ray microprobe study. J Endod 1975;1:205–10.
[4] Margelos J, Eliades G, Palaghias G. Corrosion pattern of silver points in vivo. J Endod 1991;17:282–7.
[5] Goon WWY, Lugassy AA. Periapical electrolytic corrosion in the failure of silver point endodontic restorations: report of two cases. Quintessence Int 1995;26:629–33.
[6] Mueller, HJ. In vitro tarnish and corrosion of a consolidated silver material for direct filling applications. Dent Mater 2001; 17:60–70.

[7] Vaidyanathan TK, Prasad A. In vitro corrosion and tarnish analysis of the Ag–Pd binary system. J Dent Res 1981;60:707–15.
[8] Olsson S, Berglund A, Bergman M. Release of elements due to electrochemical corrosion of dental amalgam. J Dent Res 1994;73:33–43.
[9] McDonald JR. Impedance spectroscopy. New York: Wiley-Interscience, 1987.
[10] Seitz MA, Hirthe RW, Koehler CJ. Process-monitoring via impedance spectroscopy. Mater Res Soc Symp Proc 1996;411:57–68.
[11] Boukamp BA. Equivalent circuit (EQUIVCKT.PAS). Netherlands: Department of Chemical Technolgy, University of Twente, 1988/89.
[12] Chana MS, Kuhn AT. A critique of the Tuccillo–Nielsen wheel method for tarnish testing of dental alloys. J Dent 1984;12:319–27.
[13] Tomashov ND. Theory of corrosion and protection of metals, the science of corrosion. New York: MacMillian, 1966. p. 133–363.
[14] Shoesmith DW. Kinetics of aqueous corrosion. In: Davis JR, editor. Metals handbook, ninth edition, volume 13, corrosion. Metals Park, OH: ASM International, 1987. p. 29–36.
[15] De Levie R. Electrochemical response of porous and rough electrodes. In: Delahay P, editor. Advances in electrochemistry and electrochemical engineering, vol. 6. New York: Interscience, 1967. p. 321–97.
[16] Annergren I, Thierry D, Zou F. Localized electrochemical impedance spectroscopy for studying pitting corrosion on stainless steels. J Electrochem Soc 1997;144:1208–15.
[17] Sridhar N, Dunn DS. In situ study of salt film stability in simulated pits of nickel by Raman and electrochemical impedance spectroscopies. J Electrochem Soc 1997;144:4243–53.
[18] Olsson S, Bergman M, Marek M, Berglund A. Connections between polarization curves and $\log(a_i/a_{ref})$-pe diagram. J Dent Res 1997;76:1869–78.
[19] Lide DR, editor. CRC handbook of chemistry and physics, 1997–1998, 78th ed. New York: CRC Press, 1997. p. 8-20–8-30.
[20] Hanawa T, Ota M. Calcium phosphate naturally formed on titanium in electrolyte solution. Biomaterials 1991;12:767–74.
[21] Palaghias G. The role of phosphate and carbonic acid-bicarbonate buffers in the corrosion processes of the oral cavity. Dent Mater 1985;1:139–44.
[22] Nakamoto K. Infrared and raman spectra of inorganic and coordination compounds, 4th ed. New York: Wiley, 1996.
[23] Lemaitre L, Moors M, Van Peteghem AP. A model for the corrosion behavior of dental amalgam. J Biomed Mater Res 1989;23:241–52.
[24] Lemaitre L, Moors M, Van Peteghem AP. A mechanistic study of the electrochemical corrosion of the $\gamma 2$ phase in dental amalgams. II: introduction of a model. J Oral Rehabil 1989b;16:543–8.